Drug Design, Development and Therapy

Dovepress
Taylor & Francis Group

Open Access Full Text Article

ORIGINAL RESEARCH

Design, Synthesis and Evaluation of Novel Cyclopropanesulfonamide Derivatives for the Treatment of EGFR^{C797S} Mutation in Non-Small Cell Lung Cancer

Mengxuan Wang[1,*], Zhenhong Xia[1,*], Wenyan Nie[1], Chunlong Wang[1], Haoran Nie[1], Shuai Zhang[1], Jiaqi Qiu[1], Yang Yang[1], Cuifang Yao[1], Ling Xu[2], Baijiao An[1]

[1]Shandong Technology Innovation Center of Molecular Targeting and Intelligent Diagnosis and Treatment, Binzhou Medical University, Yantai, Shandong, People's Republic of China; [2]Department of Respiratory Critical Care Medicine, Binzhou Medical University Hospital, Yantai, Shandong, People's Republic of China

*These authors contributed equally to this work

Correspondence: Ling Xu; Baijiao An, Email 1659996191@qq.com; anbj3@bzmc.edu.cn

Background: The 797S mutation in EGFR disrupts the covalent binding of third-generation inhibitors, causing drug resistance. Currently, no clinically drug fully overcomes this resistance.

Methods: We designed and synthesised a novel EGFR C797S-targeted inhibitor-**5d** by introducing structures such as cyclopropyl and sulfonamide with Brigatinib as the lead compound; we identified the target of action by ELISA and molecular docking, and tested its anti-tumor activity and safety in vivo and vitro, as well as its effects on cell cycle, apoptosis and DNA damage.

Results: It was found that there were 10 new small-molecule inhibitors and compound **5d** was identified as highly selective with low toxicity. WB confirmed **5d**'s inhibition of EGFR and m-TOR pathways. Mechanistic studies revealed **5d** induced cell cycle arrest in G2/M phase caused DNA damage and cell apoptosis, increasing apoptotic protein cleaved caspase-3 levels. It also inhibited growth in PC9 cells with an EGFR^{del19} mutation. Importantly, **5d** also demonstrated superior anti-tumor activity in vivo and was superior to the positive control Brigatinib.

Conclusion: We concluded that cyclopropylsulfonamide **5d** derivatives induce cell cycle arrest, apoptosis, and DNA damage by regulating tumor-related genes, thereby inhibiting the proliferation of C797S mutated lung cancer cells.

Keywords: NSCLC, EGFR C797S mutation, EGFR-TKIs, biological activity

Introduction

Lung cancer is the primary cause of cancer-related fatalities and can be categorized into two primary histological subtypes: non-small cell lung cancer (NSCLC) and small cell lung cancer.[1,2] NSCLC accounts for more than 80% of all lung cancer cases.[3,4] Epidermal growth factor receptor (EGFR) is a transmembrane receptor associated with multiple signaling pathways.[5,6] Analysis of sequencing data revealed a high frequency of EGFR mutations in NSCLC, and these mutated EGFR variants exhibited sustained kinase activity, thereby promoting tumor growth.[7] Currently, EGFR tyrosine kinase inhibitors (EGFR-TKIs), which have reached the fourth generation, are used to treat NSCLC.[8,9]

First-generation EGFR-TKIs, such as gefitinib[10] (Figure 1), erlotinib[11] and icotinib[12] are reversible inhibitors containing a quinazoline moiety. These drugs have shown promising results in the early stages of NSCLC treatment.[13] However, it has been reported that some patients showed signs of drug resistance after 9–14 months of treatment.[14–16] Owing to this, second-generation EGFR inhibitors were developed. Chemically, second-generation EGFR-TKIs contain unsaturated acrylamide side chains, which are responsible for their mode of action.[17] Second-generation EGFR-TKIs

Received: 12 September 2024
Accepted: 6 February 2025
Published: 27 February 2025

Graphical Abstract

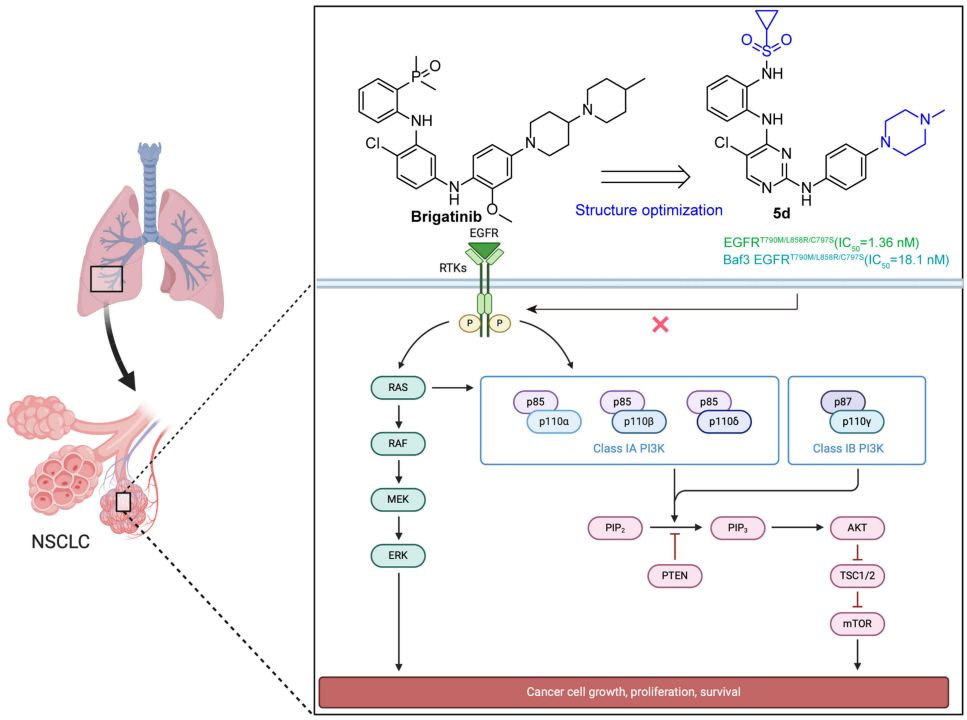

such as afatinib[18] (Figure 1) have poor selectivity, resulting in significant toxicity and limited clinical applications. Therefore, third-generation EGFR-TKIs were developed. These agents typically contain a pyrimidine-amine nucleus that maintains the acrylamide structure and is highly selective for treatment of EGFR double mutations.[19,20] In May 2015, the FDA approved the first third-generation EGFR inhibitor, osimertinib[21](Figure 1), which has become the most effective drug for patients with EGFR-sensitive and T790M-positive cancers.

Unfortunately, third-generation EGFR inhibitors may result in treatment resistance. A C797S drug resistance mutation was found in patients with EGFR^{T790M} mutations after a period of osimertinib treatment.[8] EGFR C797S, disrupting the covalent binding between the cysteine residue at position 797 of EGFR and third generation EGFR-TKIs,[22] the presence of the C797S drug resistance mutation significantly affects patient prognosis and limits effective treatment options. Extensive research is currently being conducted on fourth-generation EGFR inhibitors to prevent resistance associated with third-generation agents.[23] Strategies to overcome drug resistance can be divided into two groups according to the mechanism of drug resistance.[24] With EGFR mutations, the allosteric binding pocket, which is distant from the C797S mutation site, can be exploited. A typical example is EAI045[25] (Figure 1), an initial fourth-generation EGFR inhibitor. When EAI045 was combined with cetuximab,[26] it demonstrated inhibitory effects on EGFR$^{L858R/T790M}$ and EGFR$^{L858R/T790M/C797S}$ both in vitro and in animal models. However, it should be noted that EAI045 did not respond effectively in the absence of an anti-EGFR antibody such as cetuximab. Nevertheless, its derivative JBJ-04-125-02[27] showed improved efficacy as a standalone treatment option, although it was not effective in overcoming the 19del/T790M/C797S mutation. Additional efforts are underway to develop ATP-competitive inhibitors by modifying brigatinib, an ALK/EGFR dual inhibitor, or third-generation EGFR-TKIs.[28] In vitro and in vivo assays showed that brigatinib[29](Figure 1) has potent effects in patients with EGFR triple mutations. However, similar to that of EAI045, its anti tumor efficacy as a standalone treatment is limited. To address this limitation, modifications aimed at enhancing its potency have resulted in the discovery of a series of inhibitors that target EGFR$^{T790M/C797S}$. These inhibitors, such as BLU-945[30] and LS106,[31] have demonstrated potential anti tumor activity against osimertinib-resistant triple mutant EGFR both in vitro and in vivo. Despite this progress, no fourth-generation

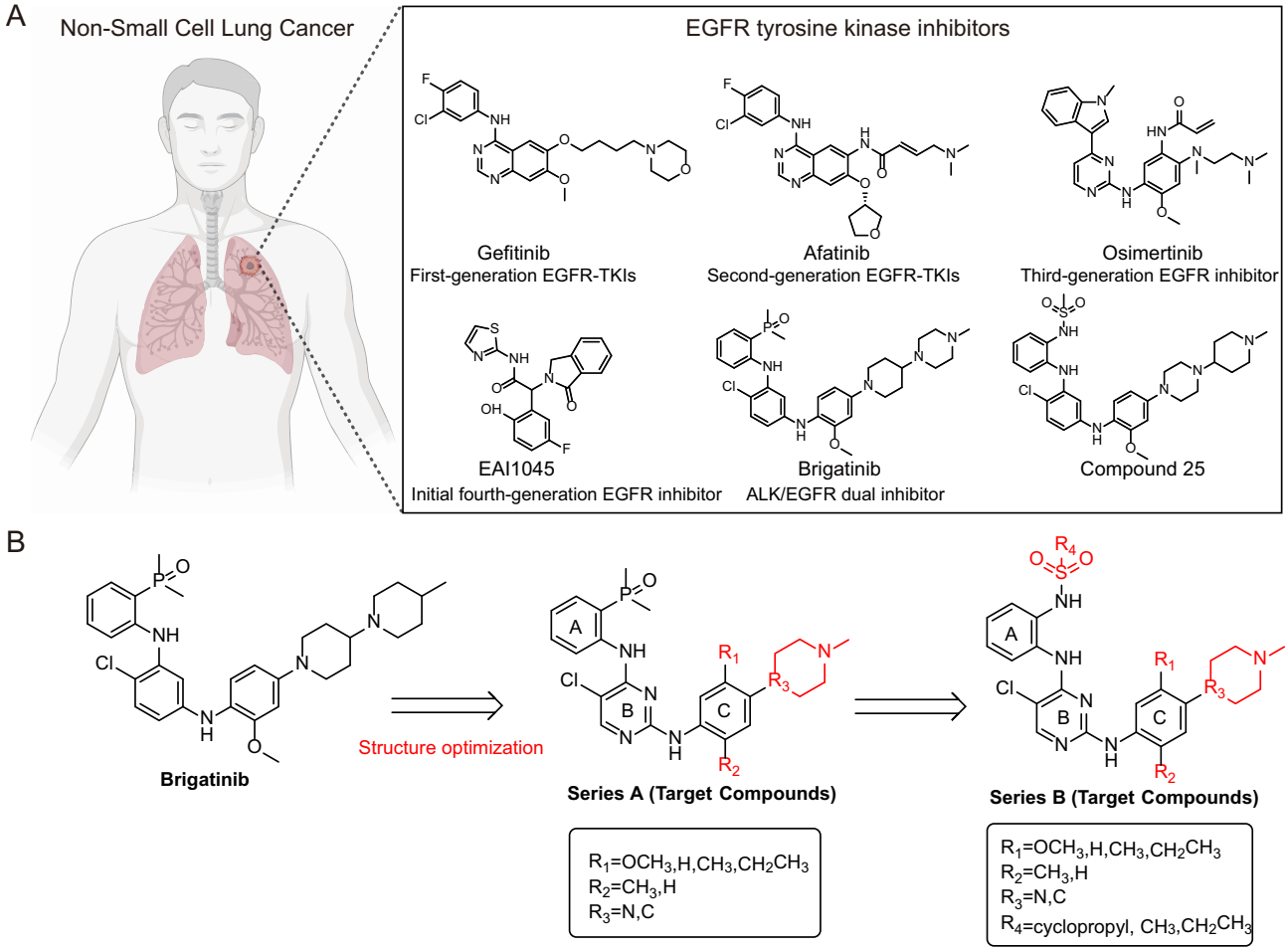

Figure 1 (**A**) Representative EGFR kinase inhibitors; (**B**) Rational design of target compounds.

EGFR inhibitors have been approved for treating C797S-resistant patients with disease progression following osimertinib therapy.[32,33] Addressing the C797S mutation is of great significance for improving treatment efficacy, overcoming drug resistance, prolonging survival, and improving patient prognosis. Consequently, there is a pressing need to develop new drugs that can effectively overcome $EGFR^{C797S}$ mutations.

Among various studies on fourth-generation EGFR triple mutation inhibitors, Lee et al reported a class of N2 and N4 diphenylpyridine-2,4-diamine derivatives containing a methanesulfonamide moiety, such as compound **25** (Figure 1), which exhibited good activity in inhibiting EGFR triple mutations in tumor cells, and thus worthy of further study.[34] In drug discovery structure activity relationship studies, small structural changes often lead to significant changes in activity. Hence, we believe that there is room for structural modification and further enhancement of the activity of these N2 and N4 diphenylpyridine-2,4-diamine derivatives. Considering the importance of cyclopropyl groups in drugs,[35] we report on the synthesis and evaluation of a series of new cyclopropanesulfonamide derivatives as fourth-generation EGFR inhibitors, including in vitro and in vivo screening for antitumor activity, along with a preliminary safety assessment. Additionally, the mechanism of action of these inhibitors on drug resistance was elucidated.

Materials and Methods

Chemistry

General Rules for Chemical Synthesis

^{1}H NMR and ^{13}C NMR spectra were recorded using TMS as the internal standard on a Bruker BioSpin GmbH spectrometer at 400 and 101 MHz, respectively. The high-resolution mass spectra were obtained using a Shimadzu

https://doi.org/10.2147/DDDT.S490303

LCMS-IT-TOF mass spectrometer. Reagents used in the synthesis were obtained commercially and used without further purification, unless otherwise specified. The reactions were monitored by thin layer chromatography (TLC) on glass-packed precoated silica gel plates and visualized in an iodine chamber or with a UV lamp. Flash column chromatography was performed using silica gel (200−300 mesh) purchased from Qingdao Haiyang Chemical Co. Ltd. The purity of the samples was determined by high-performance liquid chromatography (HPLC), conducted on a Shimadzu LC-20AT series system with a TC-C18 column (4.6 mm × 250 mm, 5 μm), and the samples were eluted with a 40:60 acetonitrile/H_2O mixture, at a flow rate of 0.5 mL/min. Full NMR spectra, HPLC chromatograms, high resolution mass spectra for target compounds are present in the Supplementary Information is the NMR, HRMS and HPLC spectra of target compounds.

The Synthesis of the Target Compounds

Synthesis of Intermediate 2

To a solution of 1.2-phenylenediamine (2.16g, 20 mmol) in 15mL of anhydrous acetonitrile, methyl sulfonic anhydride (3.83g, 22 mmol), DMAP (0.122g) and triethylamine (2.1mL) were added. The reaction was refluxed at 80°C for 8 hours. The solvent was evaporated under reduced pressure and the residue was extracted with dichloromethane (30mL*4). The solvent was removed and the crude product was purified by silica gel column chromatography (petroleum ether: ethyl acetate, 10:3, then, 2:1) afford to intermediate **2**.

Synthesis of Intermediate 4

Intermediate **2a** (2.5g, 13.4 mmol) was dissolved in 17mL of anhydrous DMF, sodium hydride (60%, 1.2g) was added at 0°C. After stirred for 15 minutes, 2,4,5-trichloropyrimidine (3.2g) in 13 mL of anhydrous DMF was added in dropwise. The ice bath was removed and the reaction was continued for 2–3 hours at the room temperature. Water 15mL was added to quench the reaction and then extracted with 30mL of ethyl acetate for 3 times. The combined organic phase was dried with anhydrous sodium sulfate, concentrated under reduced pressure to provide the crude product which was purified by silica gel column chromatography (petroleum ether: ethyl acetate, 4:1).

Synthesis of Amine Intermediates 8b-C

A solution of 4-fluoro-2-methoxy-1-nitrobenzene (3.42g, 20 mmol) in 27mL of anhydrous acetonitrile was added N-methylpiperazine (3.0g, 30 mmol), anhydrous potassium carbonate (4,41g, 32 mmol). The reaction was refluxed at 80 °C for 8–10 hours. The solvent was removed under the reduced pressure. Water 30 mL was added to the residue and then extracted with dichloromethane (50mL *2). The organic phase was dried over Na_2SO_4, and concentrate to give yellow oily for the next step without purification. The above yellow oily intermediate 5.9g was dissolved in 60mL of dichloromethane/methanol (1/1), stannous chloride (17g) and 14mL of concentrated hydrochloric acid were added. The reaction was heated at 50 °C for 4–8 hours. After the reaction is complete monitored by TCL, ammonia hydroxide and Na_2CO_3 were added to the reaction under an ice bath, filtered with diatomite, washed with dichloromethane/methanol (1/1). The organic layer was separated and the water layer was extracted with dichloromethane. The combined organic phase was dried over Na_2SO_4. The solvent was removed to afford the crude product which was purified by silica gel column chromatography (CH_2Cl_2/CH_3OH (1/1).

Synthesis of Amine Intermediate 14

A solution of 1-chloro-2-fluoro-5-methyl-4-nitrobenzene (7.0g, 37mmol) in methanol (68mL) was added anhydrous potassium carbonate (5.2g, 37.7 mmol). After refluxed at 66 °C for 4–6 hours, the reaction was filtered and removed the solvent to give the product for the use of next step directly.

The above intermediate (16g, 79.6 mmol) was dissolved in 1.4-dioxane (100mL), and then 4-pyridylboric acid (4.56g, 37 mmol), anhydrous potassium carbonate (10.2g, 74 mmol), bis triphenylphosphine palladium dichloride (0.78g, 1.11 mmol), 25mL of water were added. The reaction was refluxed at 101 °C under nitrogen for 8 hours. After the solvents were removed under the reduced pressure, dichloromethane was added. The extracts was washed with brine, dried over sodium sulfate, concentrated and purified with silica gel column chromatography (Petroleum: ethyl acetate, 4:1) to give the intermediate **11**.

To a solution of intermediate **11** in 60mL of acetonitrile, iodomethane (6.31g, 44.4 mmol) was added and the mixture was heated at 50 °C for about 4 hours. The solvent was removed to afford the crude product which was directly used for the next step without purification. The above crude product was dissolved in 200mL of methanol; sodium borohydride (8.4g, 222mmol) was added in batches under an ice bath. After the reaction finished (monitored by TLC), aqueous sodium hydroxide solution was added to adjust pH to 10–12, and the mixture was extracted with dichloromethane. The organic phase was concentrated and the crude product was purified by silica gel column chromatography (dichloromethane: methanol, 20:1) to afford the intermediate **12**.

Intermediate **12** was dissolved in a mixed solvents 50mL (dichloromethane/methanol, V/V), then 20g of stannous chloride and 10mL of concentrated hydrochloric acid were added. The mixture was heated at 50°C for 6 hours and then cooled to room temperature. Ice (20g) was added to the reaction and then sodium hydroxide (4.8g) in batches under an ice bath and stirring. The organic solvents were removed under the reduced pressure, and the residue was extracted twice with 20mL of dichloromethane. The solvent was removed in vacuum and the crude product was purified with silica gel column chromatography (petroleum/ethyl acetate 4/1, followed by dichloromethane/methanol, 10/1) to give the intermediate **13**.

To a solution of intermediate **13** (1g) in methanol (5mL), 10% palladium carbon (0.3g) was added. The reaction was pressurized at 40 Bar of hydrogen. After stirred at 50°C for 24 hours, the mixture was filtered, concentrated to afford the intermediate **14** which is directly used for the next step without purification.

Synthesis of Intermediate 16

To a solution of 2,4,5-trichloropyrimidine (10mmol, 1.82g) in DMF (25mL), (2-aminophenyl)dimethylphosphine oxide (10mmol, 1.69g), anhydrous potassium carbonate (12mmol, 1.66g), tetrabutylammonium bisulfate (1mmol, 0.34g) were added. The mixture was stirred and heat at 65 °C for 8 hours. After the reaction finished, the solvent was removed in vacuum, and the crude product was purified with silica gel column chromatography (petroleum ether: ethyl acetate in 1:1) to obtain the product.

Typical Procedure for the Synthesis of Target Products 5a-5h and 17a-17b

To a solution of intermediate **16 (**0.95g, 3 mmol) in 15 mL isopropanol, 2,2,2-trifluoroacetic acid (0.884g, 7.8 mmol), 4-(4-methylpiperazin-1-yl)aniline or 2-methoxy-5-methyl-4-(4-methylpiperazin-1-yl)aniline (3 mmol) were added. After the mixture was heated at 85 °C for 8–12 h, the solvent was removed in vacuum. Dichloromethane (50 mL*3) was added to extract the product, and then purified with silica gel column chromatography (petroleum ether: ethyl acetate in 1:1) in a yields 50–70%.

Biological Assay

Cells and Cultures

Human non-small-cell lung cancer (NSCLC) cell lines (A549 and PC-9) and human normal cells (LO2, HK2, and 293A) were purchased from the Guangzhou Jennio Biotechnology Co. LTD (Guangzhou, China). And the $BaF3^{19del/T790M/C797S}$ and $BaF3^{L858R/T790M/C797S}$ were purchased from the KYinno (Beijing, China). The NSCLC cells were cultured in RPMI 1640 medium containing 10% FBS, 100 units/mL penicillin, and 100 μg/mL streptomycin. $BaF3^{19del/T790M/C797S}$ and $BaF3^{L858R/T790M/C797S}$ were grown in RPMI 1640 containing 15% FBS. All cells were incubated at 37 °C in an atmosphere of 5% CO_2. Tests for mycoplasma contamination were negative.

ELISA Assay

Enzyme-Linked Immunosorbent Assay for mutant $EGFR^{L858R/T790M/C797S}$ and mutant $EGFR^{19del/T790M/C797S}$. Mutant $EGFR^{L858R/T790M/C797S}$ and mutant $EGFR^{19del/T790M/C797S}$ ELISA (ADANTI, USA) was used and normalized to the total EGFR content. Concentrations consisting of 6 levels from 0.005 to 5 mM were used for all of the tested compounds. Assays were performed in triplicates for each measurement using 50 μL per well in accordance with the manufacturer's instructions. Generally, the mixture of $EGFR^{L858R/T790M/C797S}$and $EGFR^{19del/T790M/C797S}$ antibody substrate, appropriate kinase (HRP labeled antibody to EGFR) and different concentrations of compounds were converged with the reaction

buffer with DMSO solution as the negative group. The kinase reaction was initiated by the addition of tyrosine kinase proteins diluted 40μL of reaction buffer solution and incubated for 30min at 37 ◦C. Dilute the concentrated washing solution in the kit into 1X, discard the solution on the enzyme plate, shake dry, fill each hole with the washing solution, leave for 30 seconds, then discard the solution, repeat 5 times, pat dry. Add color developer A (50μL) to each well, then add color developer B (50μL), gently shake and mix, hide from light for 15 minutes at 37°C. And then 50μL of stop buffer was added to stop the reaction. The IC_{50} values were calculated using the GraphPad Prism software (GraphPad Inc., La Jolla, CA, USA).

Cell Growth Assay

As described previously, the cells and the human normal cells (5×10^3 cells/well) were seeded in 96-well sterile plastic plates, incubated overnight, and then treated with the different concentrations (10, 1, 0.1, 0.05, 0.01 and 0.001 uM) drugs. After 48 h of treatment, 10 μL Cell Counting Kit-8 was added to each well and the plates were incubated for 40 min. Briefly, for the $BaF3^{19del/T790M/C797S}$ and $BaF3^{L858R/T790M/C797S}$, 1×10^4 cells were seeded in a 96-multiwell plate and the drugs and cells were cultured for a total of 48 h. Then, 10 μL Cell Counting Kit-8 was added to each well and the plates were incubated for two hours and a half. The results were representative of at least three independent experiments; the error bars signify standard deviation (SD). The IC_{50} values were calculated using the GraphPad Prism software (GraphPad Inc., La Jolla, CA, USA).

Cell Apoptosis and Cell Cycle Assay

As described previously, the $BaF3^{19del/T790M/C797S}$ and $BaF3^{L858R/T790M/C797S}$ were seeded in 6-well plates (3×10^4 cells/well) and incubated in the presence or absence of compound 5d for the cell apoptosis assay, cells were harvested and incubated with 5 μL of Annexin-V/FITC (Keygen Biotech, China) in binding buffer (10 mM HEPES, 140 mM NaCl, and 2.5 mM $CaCl_2$ at pH 7.4) at room temperature for 15 min. PI solution was then added to the medium for another 10 min-incubation. Almost 10,000 events were collected for each sample and analysed by flow cytometry (Beckman Coulter, Epics XL). For the cell cycle assay, the cells were collected and rinsed once with PBS before overnight fixation with pre-cooled 70% ethanol at −20 °C. The fixed cells were washed twice with cold PBS and incubated in the dark at 37°C with 10μL RNAse A and 50 μg/mL PI staining solution for 30 min. The data regarding the number of cells in different phases of the cell cycle were analysed using EXPO32 ADC analysis software.

Assays for DNA Damage

The $BaF3^{19del/T790M/C797S}$ and $BaF3^{L858R/T790M/C797S}$ were seeded in 6-well plates (2×10^4 cells/well) and incubated in the presence or absence of compound **5d** for 24 h. Almost 10,000 events were collected for each sample and analysed by flow cytometry (Beckman Coulter, Epics XL). For the DNA Damage assay, the cells were collected and rinsed once with PBS. Then fixation with 4% PFA (Beyotime, China) at room temperature. The cells were washed three times in PBS for 5 minutes each, and then incubated with DNA Damage Assay Kit by γ-H2AX Immunofluorescence (Beyotime, China). Dye with DIPA from the kit for 15min. Leica SP5 confocal laser scanning microscopy (Leica Microsystems, Buffalo Grove, USA) was used for immunofluorescence imaging.

Western Blot Analysis

After treatment with **5d** or osimertinib for 4–48 h, cells were washed with PBS, then cleaved on ice with RIPA (Beyotime, China) containing 1% protease inhibitor and phosphorylase inhibitor, centrifuged at 12000 rpm for 15 min to collect proteins. After the protein concentration was determined by BCA kit (Beyotime, China), the samples were packaged and boiled. The protein was coated on 10% SDS-PAGE glue and then transferred to PVDF (Merck, Germany) membrane. 5% skim milk powder was enclosed with PVDF membrane and incubated at 4°C overnight. Then membranes were then incubated with HRP-conjugated secondary antibodies at room temperature and developed with luminescent solution ((Pierce, Rockford, IL, USA). P-EGFR (1:1000;3777T, Cell signaling), EGFR (1:1000;4267T, Cell signaling), p-AKT (1:1000;AF6261, affinity), AKT (1:1000;GR100134-1, Abcam), p-ERK (1:1000;AF1015, affinity), ERK (1:1000;4695T, Cell signaling), GAPDH (1:1000;10,494-1-AP, proteintech), P70S6K (1:1000;9202S, Cell signaling),

p-P70S6K (1:1000;9234S, Cell signaling), cleaved caspase-3 (1:1000;9661L, Cell signaling), PI3K (1:1000; AF6241, affinity), p-MER (AF8443, affinity), P-PI3K (1:1000; AF3242, affinity), AMPK (1:1000; 9158, Cell signaling), P-AMPK (1:1000; 2537, Cell signaling), β-actin (1:1000;A5441, Sigma). Full and uncropped Western blots are presented in Figure S1 of original Western blot. Protein statistical analysis diagram are presented in Figures S2 and S3.

Acute Toxicity Test

Female and male Kunming mice (12 mice each, 18 ~ 25 g) were purchased and housed at the SPF(BEIJING) BIOTECHNOLOGY CO., in pathogen-free condition, maintained at constant room temperature and fed a standard rodent chow and water. The mice were randomly divided into experimental group and control group. The animals were fasted overnight before drug administration, and the drug was administered by tail vein injection at a constant volume of 0.4 mL/20 g (concentration of the administered drug: 20mg/kg, 40mg/kg, 80mg/kg, and 100mg/kg) with observations of body weight and mental state at 24h, 48h, and 72h post-administration.

Xenograft Tumor Model

Male BALB/c nude mice, 3–4 weeks old were purchased from spfbiotech (SPF(BEIJING)BIOTECHNOLOGY CO., LTD., Beijing, China) and allowed to acclimate for 1 week. Animal care was in accordance with the institutional animal care guidelines. All animal experiments were approved by the Animal Ethics Committee of the Institutional Ethics Review Board of Binzhou Medical University. Logarithmic growth of 1×10^7 cancer cells/mL were re-suspended in 1640 medium without FBS. Then, 200 uL cell suspension was injected subcutaneously into the right side of each mouse. After the tumor had formed a hard mass, the tumor volume was measured every two days. When the tumor volume reaches 150–200 mm^3, the xenograft tumor-bearing nude mice were randomly allocated to Four groups (vehicle-treated, **5d**-70 mg/kg, **5d**-100 mg/kg and osimertinib-100mg/kg) with 7 mice per group. Each group was dosed by intragastric administration (ig) for 9 days. Tumor volume and mouse body weight were recorded after daily administration. At the end of the observation period, the animals were euthanized by cervical dislocation and the tumor bulks were peeled off conformed to the Guide for the Care and Use of Laboratory Animals as published by the US National Institutes of Health (NIH Publication No. 85–23, revised 1996) and approved by the Institutional Ethics Review Board of Binzhou Medical University.

Immunohistochemistry

Immunohistochemistry (IHC) detected the expression of Ki67, P-EGFR in tumor tissue. The tumor tissue paraffin sections were deparaffinized, and endogenous peroxidase activity was blocked by incubation with 3% H_2O_2. The blocked sections were incubated with Ki67 antibody (1:500; proteintech, 27309-1-AP), P-EGFR antibody (1:500; 4267T, Cell signaling) at 4°C overnight and then sequentially incubated with a biotin-labeled secondary antibody. The sections were then stained with 3.3′-diaminobenzidine. Finally, the sections were counterstained using hematoxylin and fixed. For each section, three fields of view were randomly selected and photographed under 400× magnification.

HE Staining

The morphological changes of heart, liver, spleen, lung and kidney were detected by HE staining. Paraffin sections of tissue were dewaxed, reversed stained and fixed with eosin and hematoxylin. 3 fields of view were randomly selected for each profile and shot at 400×.

Cell Morphology

Human normal cells LO2, HK2, and 293A were placed in a six-well plate overnight, and then treated with 10 μM compound **5d** for 48 h. The morphological changes were observed under a 400X microscope.

Statistical Analysis

All experiments were repeated three times independently unless specifically indicated. The data was analyzed by GraphPad Prism 7 software. The data was shown as mean±SD and one-way ANOVA Tukey ‘s multiple comparison

test was used to determine the levels of significance between comparison samples. Results with $p < 0.05$ were considered statistically significant; results with $p < 0.01$ were considered extremely significant.

Results

Synthesis of Target Compounds

The synthetic route for the target compounds **5a–5h** is shown in Figure 2. First, benzene-1,2-diamine **1** was reacted with sulfonic anhydride or cyclopropane sulfonyl chloride to provide intermediate **2**, followed by the reaction of 2,4,5-trichloropyrimidine **3** with sodium hydride to afford **4**. Intermediate **4** was reacted with aniline derivatives **8** or **14** to give sulfonamide moieties containing the target compounds **5a–5h**.

Aniline derivative **8** was synthesized using fluorinated nitrobenzene derivative **6** as the starting material. Compound **6** was reacted with 1-methylpiperazine in the presence of sodium carbonate and then reduced with tin dichloride to give **8** in good yield. In contrast, 1-chloro-5-fluoro-2-methyl-4-nitrobenzene was reacted with methanol in the presence of

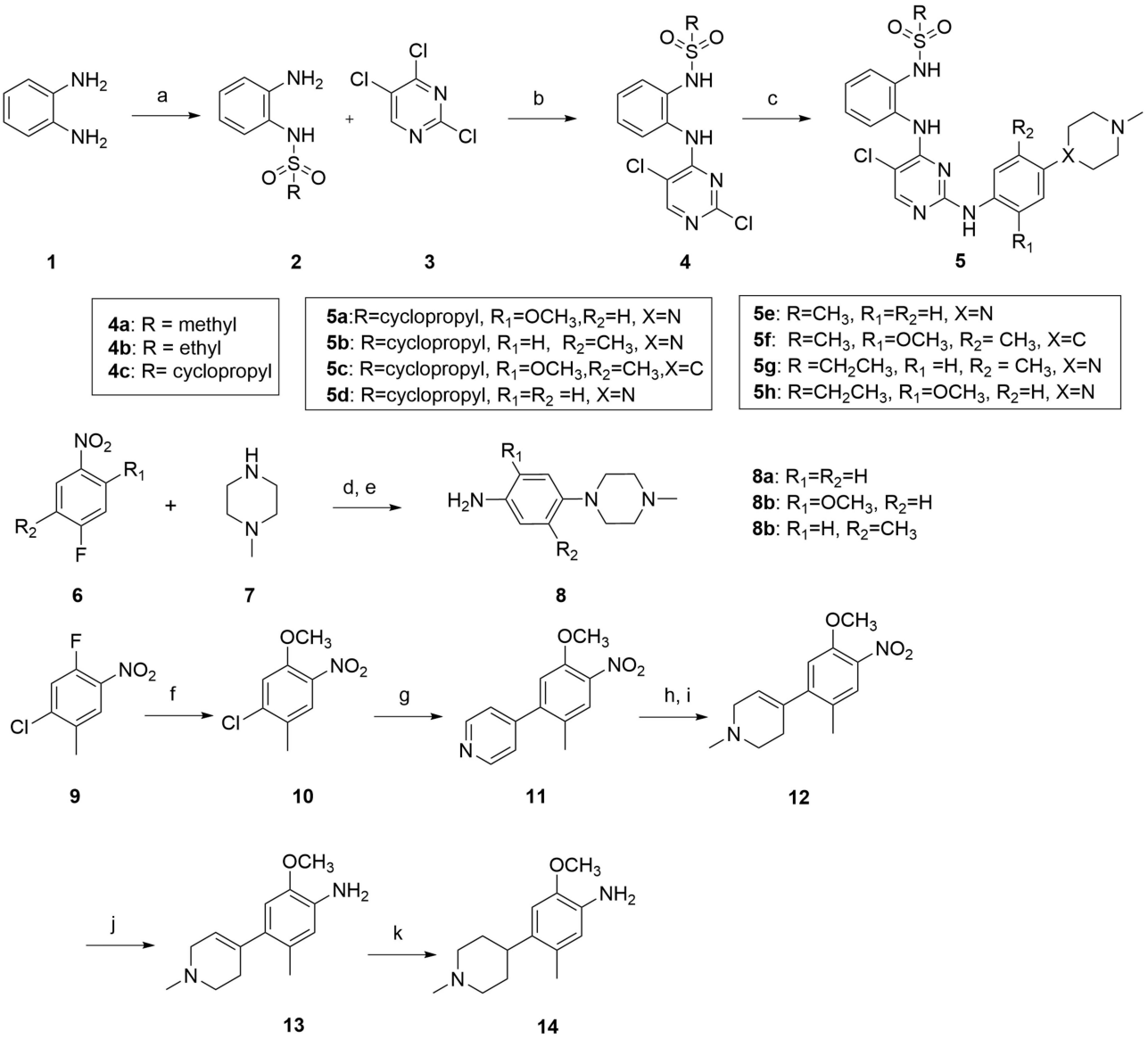

Figure 2 The synthesis route of target compounds **5a-5h**. (**a**) NaH/DMF, 0°C. (**b**) Alkyl or cyclopropylsulfonyl chloride, DIPEA. (**c**) Aniline derivatives **8**, CF_3COOH, isopropanol, 80°C, 8–24h. (**d**) K_2CO_3/CH_3CN, 80°C, 8–10h. (**e**) $SnCl_2$. (**f**) K_2CO_3/CH_3OH, reflux, 6h. (**g**) pyridin-4-ylboronic acid, K_2CO_3/1,4-dioxane/$Pd(PPh_3)_2Cl_2$. 100° C, 8h. (**h**) CH_3I/CH_3CN, 50°C, 5h. (**i**) NaBH4/CH_3OH, 0°C to rt. (**j**) $SnCl_2$. (**k**) H_2, Pd/C.

sodium carbonate to afford the methyl ether derivative **10**. The coupled reaction of **10** with pyridin-4-ylboronic acid, catalyzed by $Pd(PPh_3)_2Cl_2$, resulted in intermediate **11**. Compound **11** was reacted with iodomethane and was then reduced with sodium borohydride to afford **12**. The reduction of **12** with tin dichloride and, finally, hydrogenation in the presence of Pd/C gave aniline derivative **13**.

The target compounds **17a** and **17b** were synthesized via the route shown in Figure 3. Commercially available (2-aminophenyl)dimethylphosphine oxide **16** was reacted with 2,4,5-trichloropyrimidine to produce intermediate **17**. In the presence of 2,2,2-trifluoroacetic acid, the reaction of **17** with aniline derivatives **15** or **8a** smoothly afforded target compounds **17a** and **17b**.

Antitumor Activity of Target Compounds

To test if the target compounds inhibit the C797S mutation, we measured their IC_{50} using a Ba/F3 cell line expressing the $EGFR^{C797S}$ mutant with a CCK8 assay, followed by an ELISA to assess their activity against the EGFR C797S mutant kinase (Table 1). As shown in Table 1, most of the target compounds exhibited good to excellent EGFR ^{C797S} Kinase inhibitory activities, with IC_{50} values ranging from 1.12 to 7.928 nM. Among them, compound **5d**, which possesses sulfonamide groups, exhibited the best kinase inhibition activity, with IC_{50} values of 1.37 nM and 1.12 nM. Further structure-activity analysis indicated that the substituents on the aromatic ring had a significant impact on activity. Compound **5a**, with methoxy groups such as R_1, exhibited lower activity (7.39 and 6.63 nM) than its analog **5d** (R_1= H; 1.37 and 1.12 nM), implying that the methoxy group at the R_1 position was unfavorable for activity. The R group of the sulfonamide moiety also had an impact on activity, and the use of cyclopropyl as the R group (**5d**) seemed to be better than the use of methyl groups (**5e**, 4.83, and 3.08 nM). However, there was minimal impact on activity if the R_2 group was a methyl or hydrogen group. Compounds **17a** and **17b**, which are dimethylphosphine oxide derivatives, exhibited relatively lower activities (3.21 to 6.81 nM, respectively) than compound **5d**. Concurrently, we selected the EGFR kinase inhibitor Osimertinib, known for its resistance to the EGFR C797S mutation, and the ALK kinase inhibitor Brigatinib, which exhibits inhibitory activity against the EGFR C797S mutation, as positive controls. The results indicated that the anti-proliferative efficacy of all tested compounds against the EGFR C797S kinase exceeded that of the positive control Osimertinib, with IC_{50} values ranging from 45.788 nM to 84.331 nM, and was comparable to Brigatinib, which exhibited IC_{50} values ranging from 4.126 nM to 6.587 nM. Notably, the compound **5d** demonstrated superior performance relative to the positive control Brigatinib. Overall, the observed trend in the antiproliferative effects of the synthesized compounds on the two EGFR triple mutant cell lines is consistent with their kinase inhibitory activity. The best results were obtained with **5d**, a cyclopropanesulfonamide derivative, which had 18 and 25 nM IC_{50} values for Baf3-$EGFR^{L858R/T790M/C797S}$ and Baf3-$EGFR^{19del/T790M/C797S}$ cell lines, respectively. Because of the excellent results of compound **5d** in both kinase inhibitory and antiproliferation activities, it was selected for further study.

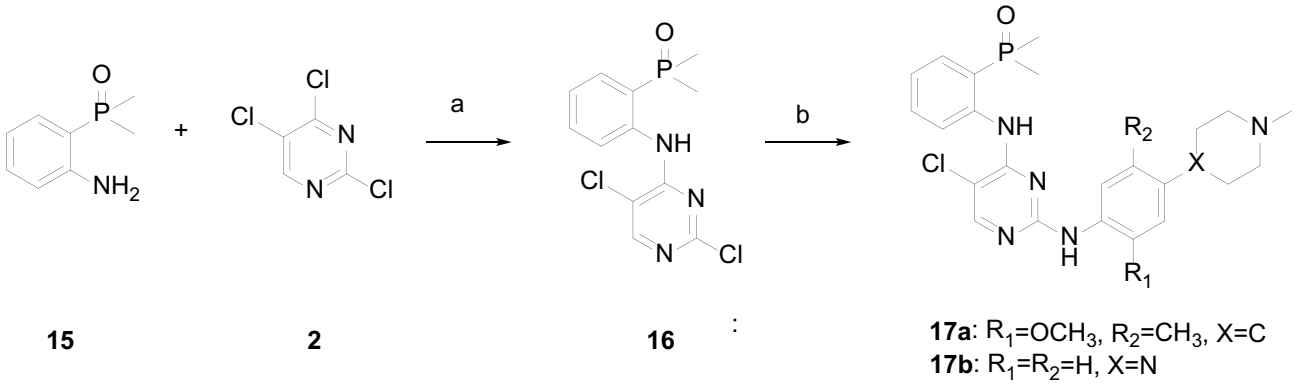

Figure 3 The synthesis route of target compounds **17a-17b**. (**a**) K_2CO_3, Tetrabutylammonium hydrogen sulfate/DMF. (**b**) Aniline derivatives **15** or **8a**, CF_3COOH, isopropanol, 85°C, 8–12 h. Table 1 The target compound against C797S mutant cells and kinase activity. Values represent the means of at least three separate determinations and are expressed as mean±SD. n = 3.

https://doi.org/10.2147/DDDT.S490303

Table 1 The Target Compound Against C797S Mutant Cells and Kinase Activity

	IC_{50} (nM)			
	$EGFR^{L858R/T790M/C797S}$	**$EGFR^{19del/T790M/C797S}$**	**Baf3-$EGFR^{L858R/T790M/C797S}$**	**Baf3-$EGFR^{19del/T790M/C797S}$**
5a	7.396±0.086	6.631±0.117	748±38.2	691±64.1
5b	2.018±0.045	3.122±0.016	36.2±0.77	22.3±0.92
5c	7.928±0.042	5.624±0.011	154±36.2	405±38.3
5d	1.365±0.008	1.124±0.003	18.2±0.71	25.4±0.54
5e	4.837±0.033	3.081±0.014	30.3±0.81	44.3±0.23
5f	4.108±0.074	4.122±0.052	213±112	360±34.4
5g	4.328±0.036	2.124±0.041	47.2±0.12	44.2±0.11
5h	4.391±0.050	2.137±0.011	586±41.6	611±11.7
17a	6.812±0.039	4.281±0.033	253±11.4	339±27.8
17b	3.211±0.110	5.268±0.180	66.2±3.27	59.2±2.11
Osimertinib	84.331±0.011	45.788±0.033	872±11.2	821±2.38
Brigatinib	4.126±0.028	6.587±0.017	426±18.7	378±14.5

Effect of 5d on EGFR ^{C797S} Protein

In order to further clarify the effects of the optimal compounds on EGFR proteins and the EGFR signalling pathway, we next performed an in-depth analysis of the interaction of **5d** with the $EGFR^{L858R/T790M/C797S}$ (PDB: 6LUB),[36] firstly by molecular docking assays (Figure 4A). The binding patterns of the kinase and ligands showed some similarities. The ligands bound to the hinge region and formed hydrogen bonds with MET-793. The N-methylpiperazine group of the compounds extended outward, forming a salt bond with Glu-804. Both proteins bound to the ATP-binding pocket of $EGFR^{L858R/T790M/C797S}$, confirming that they are ATP-competitive inhibitors. In addition, **5d** formed hydrogen bonds with LYS-745. Therefore, the inhibitory effect of **5d** on $EGFR^{L858R/T790M/C797S}$ cells was greater than that of brigatinib. Next, we verified their effects on intracellular protein expression using WB analysis, as shown in the Figure 4B, the expression level of phosphorylated proteins of the EGFR signalling pathway was significantly decreased after dosing. In addition, the phosphorylated proteins ERK downstream of EGFR also showed a trend of down-regulation, which indicated that the target compounds inhibited the activation of the EGFR signalling pathway, thus significantly attenuating the proliferation ability of the cells. Moreover, EGFR activates the PI3K/Akt/m-TOR signaling pathway, leading to cell growth and proliferation in NSCLC.[37] Therefore, we investigated the effect of **5d** on the expression of phosphorylated proteins in the m-TOR signaling pathway. As shown in Figure 4C, after inhibition of the EGFR signaling pathway, the PI3K/AKT/m-TOR signaling pathway was arrested. Together, these findings suggest that compound **5d** inhibits the EGFR and m-TOR signaling pathways to regulate tumor cell proliferation.

Compound 5d Caused EGFR ^{C797S} Cell Apoptosis

In order to determine whether the **5d** reduction in cell viability was due to apoptosis, flow cytometry and WB were used to evaluate the mechanism of cell death induced by compound **5d** in detail. First, flow cytometry demonstrated that **5d** promoted apoptosis in a dose-dependent manner (Figure 5A and B). Moreover, the expression of the cleaved caspase-3 protein (CC3) of the apoptotic pathway was validated by Western blot analysis, which revealed that the expression of the apoptotic protein cleaved caspase-3 was significantly increased in Baf3-EGFR C797S cells after treatment for 24h with **5d** at different concentrations (Figure 5C). In summary, compound **5d** binds well to the C797S protein, increases the expression of apoptosis-related proteins in C797S mutant cells, and causes apoptosis, thus playing an antitumor role.

Compound 5d Induced Cell Cycle Arrest

In order to confirm whether **5d** inhibits cell proliferation by inducing cell cycle arrest, flow cytometry was performed. The results, as shown in the Figure 6A–C, in $EGFR^{L858R/T790M/C797S}$ cell lines, small doses administration of the 5d compound caused the cell cycle to be blocked in the G0/G1 phase, and as the drug concentration was increased, the cell

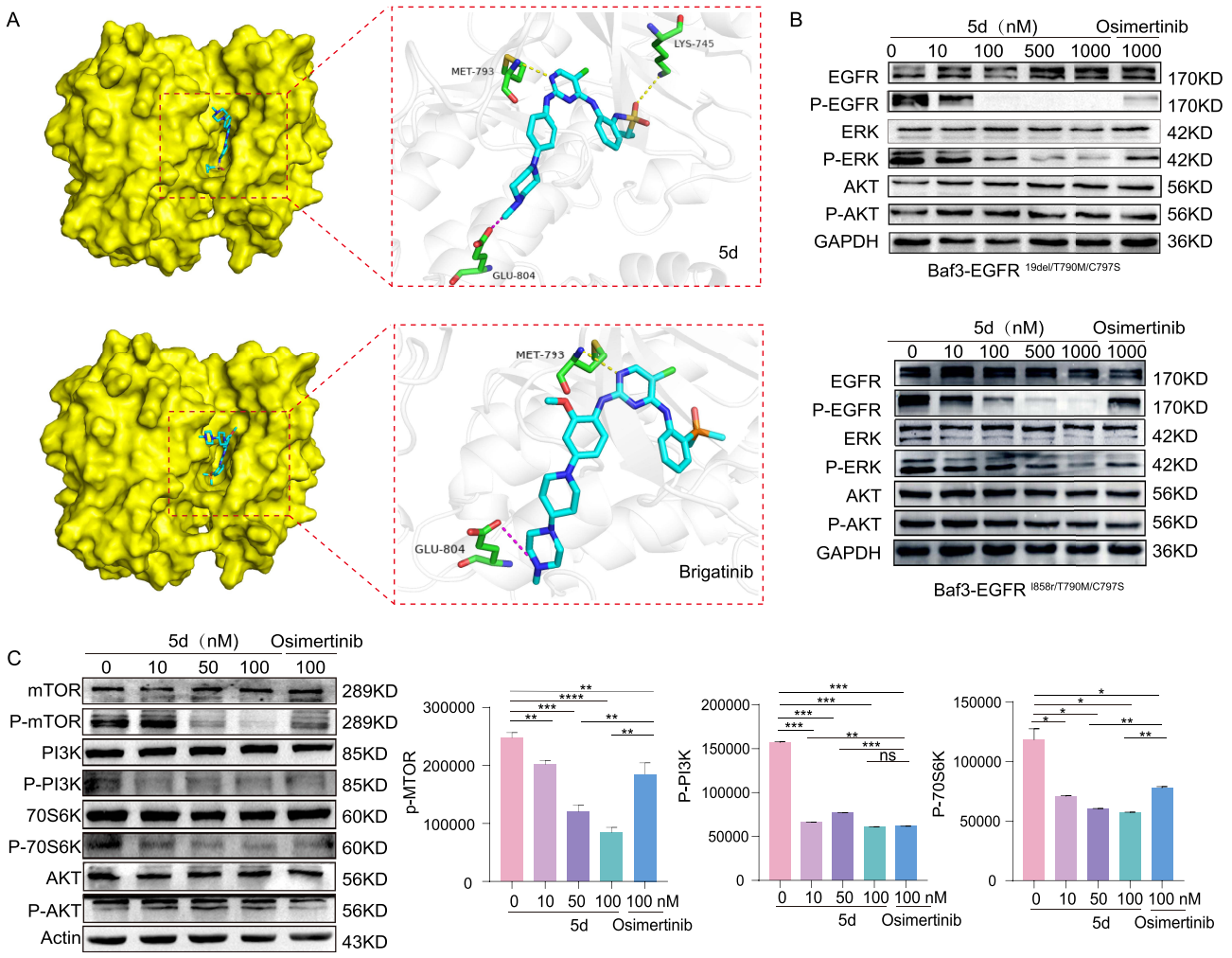

Figure 4 Molecular docking and protein regulation of Ba/F3-EGFR ^{C797S} cells by **5d**. (**A**) Docking structures of **5d** or Brigatinib with EGFR $^{L858R/T790M/C797S}$; Compound **5d** for 12 h on EGFR (**B**) and m-TOR (**C**) signalling pathways. Data are represented as mean ± SD. n = 3. ns >0.05, *p < 0.05, **p < 0.01, ***p < 0.001, ****p < 0.0001.

cycle was blocked in the G2/M phase, whereas the positive control osimertinib caused the large dose to be blocked only in the G0/G1 phase (Figure 6D). In order to verify whether cell cycle-related proteins were involved in 5d-induced cell cycle arrest, Western blotting was performed (Figure 6E). CDK1 and Cyclin B1 are major cells cycle regulators during the transition from G2 to M phase.

Compound 5d Induced DNA Damage

It is becoming increasingly important to target the DNA damage response pathway in cancer therapy. To this end, we investigated whether **5d** caused DNA damage. The initial cellular reaction to DNA double-strand breaks (DSBs) entails the phosphorylation of histone H2AX, leading to the emergence of γ-H2AX at sites of DNA damage.[38,39] Consequently, γ-H2AX may function as a marker of DNA injury. Immunofluorescence was used to investigate whether compound **5d** induced DNA damage. As depicted in Figure 7A, the level of γ-H2AX substantially increased following treatment with compound **5d**, suggesting that this compound can induce DNA damage. Subsequent WB experiments similarly verified that **5d** induced the accumulation of γ-H2AX protein (Figures 7B). As shown above, **5d** inhibits cell cycle progression by inducing DNA damage and can induce apoptosis in C797S mutant cells.

https://doi.org/10.2147/DDDT.S490303

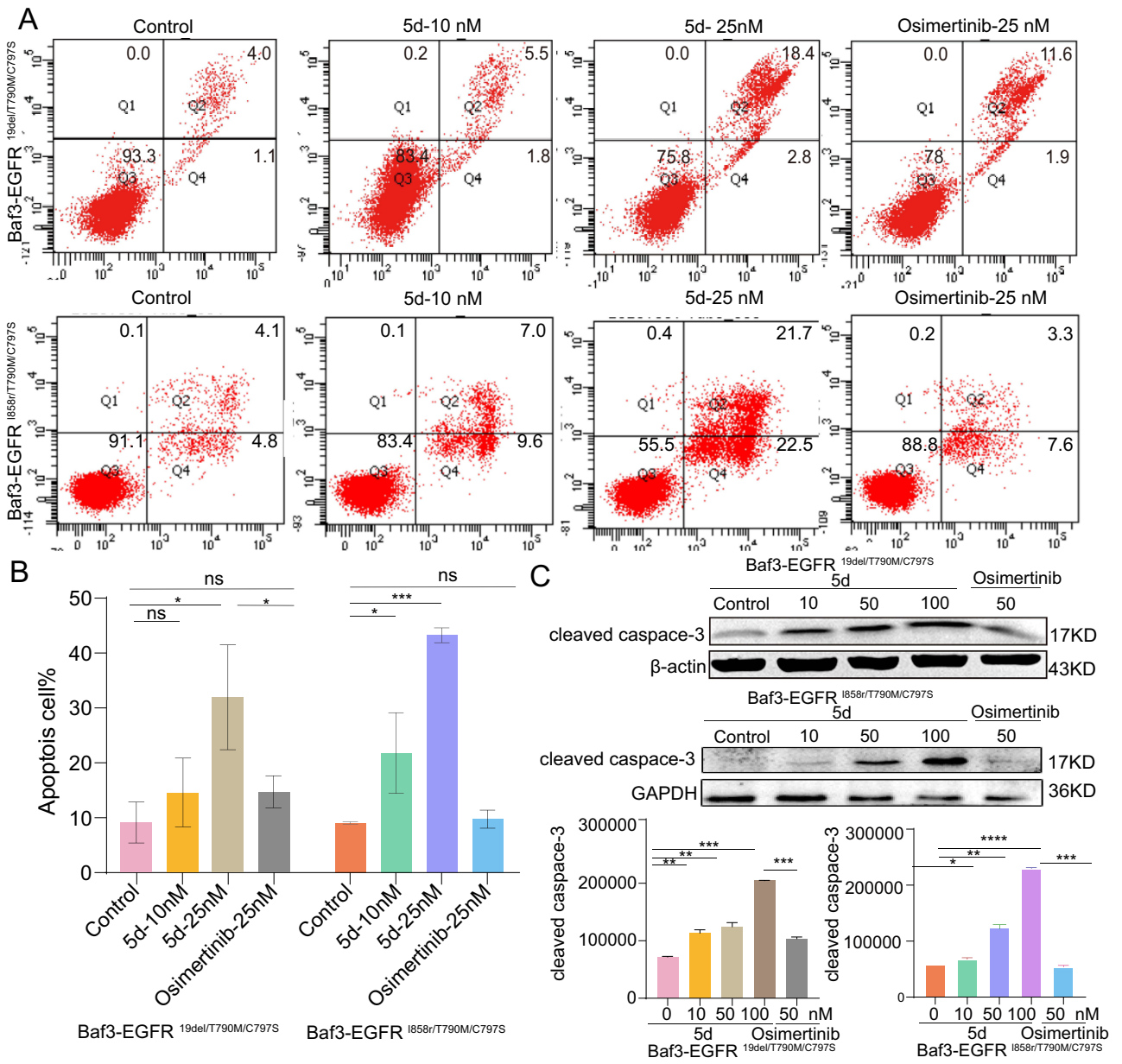

Figure 5 The compound **5d** promotes cell apoptosis.(**A**) Effect of **5d** for 24h on apoptosis in different cells; (**B**) Apoptotic cell data statistics; (**C**) Effect of **5d** for 24h on the apoptotic protein cleaved caspase-3 protein in different cells. Data are represented as mean ± SD. n = 3. ns >0.05, *p < 0.05, **p < 0.01, ***p < 0.001, ****p < 0.0001.

Compounds Inhibiting Cancer Cell Lines Harboring the EGFR^{19del} Construct

Patients with non-small cell lymphoma often have more than one EGFR kinase mutation. Therefore, EGFR inhibitors that inhibit two or more mutations are clinically important. To determine whether the synthesized compounds can inhibit cancer cell lines with other EGFR mutations, we selected PC9 tumor cells that possessed EGFR^{19del} mutations for the assay, with A549 cells (EGFR wild type) serving as the control. As shown in (Figure 8A, Table S1), most of the compounds exhibited very good anti-proliferation activity against PC9 cells, with IC_{50} values ranging from 0.011 to 0.158 μM. Among them, the optimal compound **5d** had an IC_{50} of 0.0156 μM, which was approximately the same against EGFR$^{L858R/T790M/C797S}$ cells. Meanwhile, we evaluated the morphological effects (Figure 8B) of the compound **5d** on PC9 cells. The results showed that observed cell morphology exhibited changes. Conversely, the compounds exhibited marginally reduced activity in EGFR wild-type A549 cells (Figure 8C, Table S1), indicating a degree of selectivity and implying a favorable safety profile. To substantiate the safety of the compound **5d**, we assessed the anti-proliferative

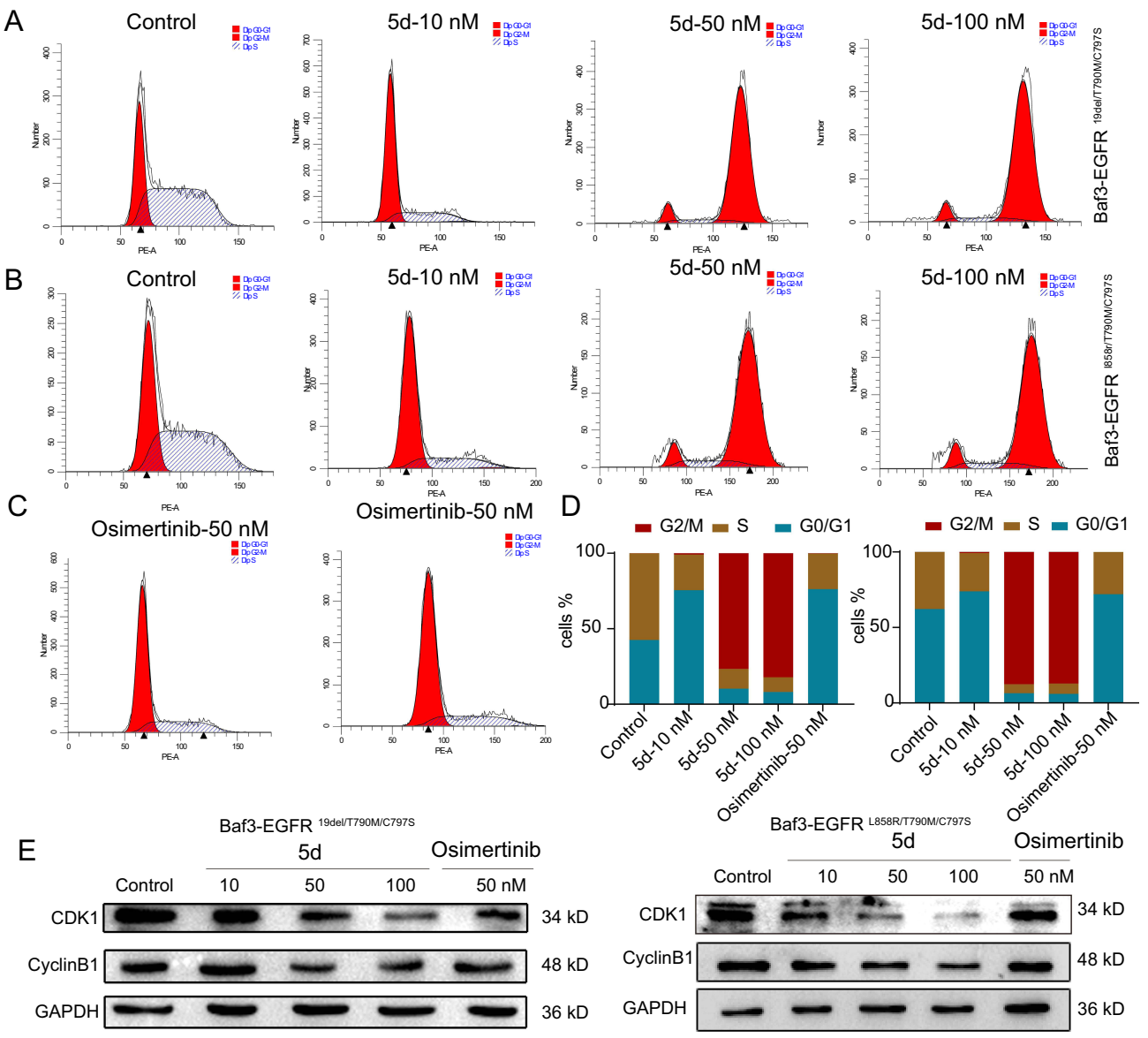

Figure 6 Compound **5d** blocks the cell cycle. Baf3-EGFR$^{L858R/T790M/C797S}$ (**A**) and Baf3-EGFR$^{19del/T790M/C797S}$ (**B**) cells were blocked from entering the G2/M phase by compound **5d**; (**C**) Baf3-EGFR$^{L858R/T790M/C797S}$and Baf3-EGFR$^{19del/T790M/C797S}$ cells were blocked from entering the G2/M phase by Osimertinib; (**D**) Cell cycle statistical analysis diagram; (**E**) Regulation of G2/M phase protein by **5d**.

effects of compound **5d** on normal cell lines LO2, HK2, and 293A. The findings, presented in Figure 8D and Table S2, demonstrated that compound **5d** exhibited low cytotoxicity in normal human cells relative to cancer cells. This outcome further supports the notion that the compound possesses a favorable safety profile.

In vivo Antitumor Activity of Compound 5d

Due to its strong ability to inhibit cell growth in a lab setting, **5d** was tested in mice for its effectiveness in fighting tumors. In acute toxicity experiments, intravenous administration of the **5d** at doses of 20mg/kg, 40mg/kg, 80mg/kg, and 100mg/kg to mice, with observations of body weight and mental state at 24h, 48h, and 72h post-administration. It was observed that mice administered the highest dose did not exhibit a decrease in body weight and maintained a good mental state. Acute toxicity experiment showed that doses under 100 mg/kg were safe. Mice with tumors were given 5d or saline daily until the average tumor volume in the control group reached 1000mm³ and the experiment ended after 9 days. The results are shown in Figure 9A–C, the **5d**-70 mg/kg and **5d**-100 mg/kg groups exhibited good in vivo results, with Tumor

https://doi.org/10.2147/DDDT.S490303

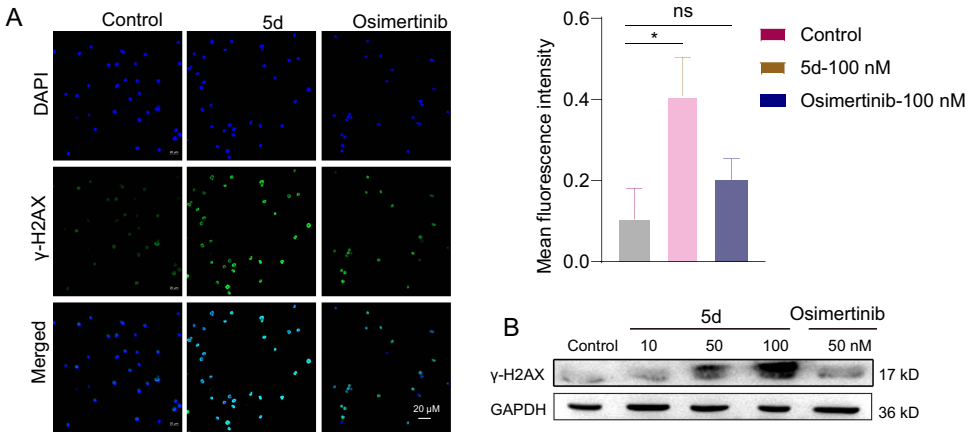

Figure 7 Compound **5d** causes DNA damage. (**A**) Immunofluorescence detection of γ-H2AX expression in C797S mutant cells (scale bar, 25 μm; ns >0.05, *p < 0.05). (**B**) Expression of γ-H2AX was determined by Western blot. Data are represented as mean ± SD. n = 3.

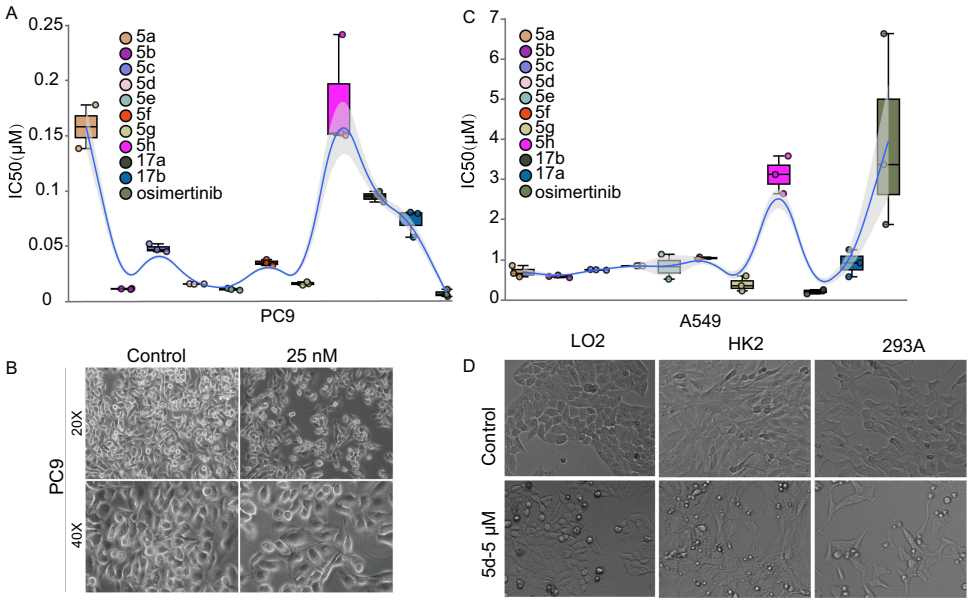

Figure 8 The impact of the compound on tumor and normal cells. (**A**)The antiproliferative activity of the compound against PC9 tumor cells over a 48-hour period; (**B**) The morphological effects of the compound on PC9 cells after 48 hours; (**C**) The antiproliferative activity of the compound against A549 tumor cells over a 48-hour period; (**D**) The morphological effects of the compound on normal cells after 48 hours.

Growth Inhibition value (TGI, TGI=(1-tumor weight of treated /tumor weight of control) *100%;). TGI rates of 45.2% and 55.7%, respectively, compared with osimertinib (TGI=13.5%) and Brigatinib (TGI=38.2%). To further determine the inhibitory effect of compound **5d** on tumor growth, we performed IHC staining to evaluate the tumor expression levels of Ki67 and p-EGFR derived from Baf3-EGFR$^{19del/T790M/C797S}$. As indicated in Figure 9D, Ki67 and p-EGFR expression in the **5d** treatment groups was lower than that in the control group. Notably, during the treatment period, the body weights of the mouse in the **5d** treatment groups did not differ significantly from those in the control group (Figure 9E), suggesting that **5d** was not significantly toxic and met drug safety requirements. Furthermore, we stained the heart, liver, spleen, lungs, kidneys, and tumor tissues of the mice with hematoxylin and eosin (H&E) to evaluate toxicity in vivo. The staining results revealed that **5d** did not cause significant organ damage after repeated administration (Figure 9F). Together, these results suggest that **5d** has potent antitumor activity while maintaining an excellent safety profile.

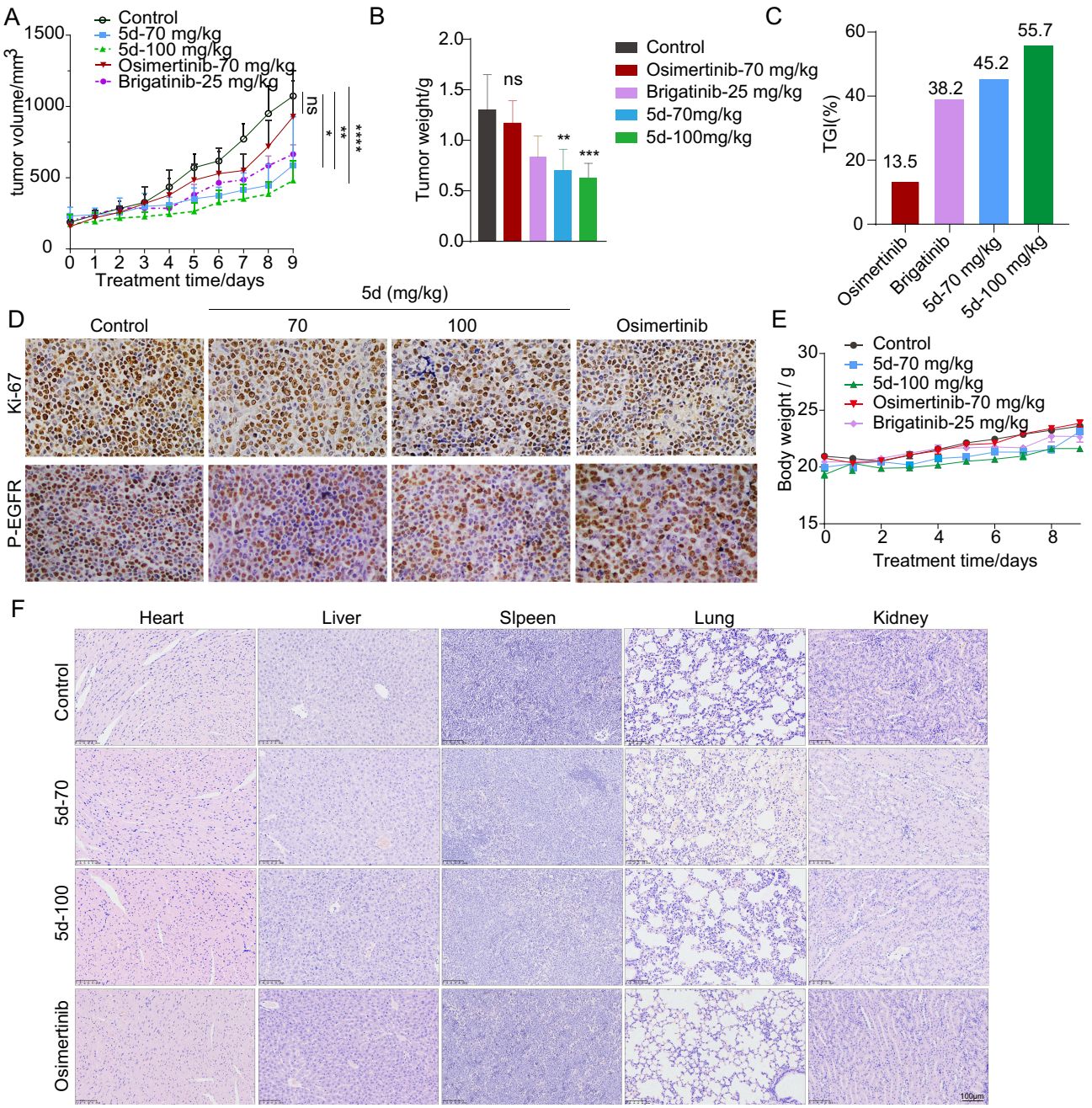

Figure 9 Efficacy and safety of compounds in vivo. (**A**) In vivo tumor growth inhibition curves; (**B**) Statistics of tumor weight in each group of mice; (**C**) The TGI values of each drug administration group were calculated based on the tumor weight, TGI=(1-tumor weight of treated /tumor weight of control) *100%; (**D**) Immunohistochemical analysis of the transplanted tumors from each group of orthotopic transplantation mice; (**E**) Alteration of body weight of mice of each group; (**F**) HE staining analysis of the main organs. Data are represented as mean ± SD. n = 7. ns >0.05, *p < 0.05, **p < 0.01, ***p < 0.001.

Discussion

Among lung cancer cases, NSCLC accounts for more than 80%. A high frequency of EGFR mutations in NSCLC and promote tumor growth. The marketed EGFR inhibitors, such as Gefitinib, Afatinib, and Osimertinib, have demonstrated successful efficacy in the treatment of NSCLC patients with EGFR mutations. However, prolonged usage of these drugs often leads to the development of drug-resistant mutations, particularly in C797S mutation after the administration of Osimertinib, resulting in a significant reduction in effectiveness. The C797S mutation is the replacement of cysteine by serine at the 797 position of EGFR. This mutation causes third-generation EGFR covalent inhibitors to lose their ability

https://doi.org/10.2147/DDDT.S490303

to covalently bind to EGFR, thus triggering resistance. Conventional EGFR inhibitors such as gefitinib and osimertinib are unable to bind to the mutated EGFR, thus failing to inhibit tumor growth. Therefore, the discovery of the C797S mutation is a major challenge for EGFR-positive lung cancer patients.

EAI045,[25] an initial fourth-generation EGFR inhibitor, usually combined with cetuximab.[26] However, EAI045 did not respond effectively when standalone. Its derivative JBJ-04-125-02[27] showed better efficacy when used alone, but it was ineffective in overcoming the 19del/T790M/C797S mutation.

Brigatinib (an ALK/EGFR dual inhibitor)[29] has a potent effect on patients with EGFR triple mutations. However, brigatinib alone has limited antitumor effects. To address this problem, a series of novel inhibitors based on brigatinib have been designed and developed, such as BLU-945[30] and LS106.[31] Although there has been some progress with fourth-generation EGFR inhibitors, no fourth-generation EGFR inhibitors have been approved for the treatment of C797S-resistant patients with disease progression following osimertinib treatment.

The acquired resistance of third-generation EGFR inhibitors, represented by Osimertinib, is an urgent clinical issue. Inspired by cyclopropyl ring in many drug molecules that addresses multiple road blocks such as enhancing potency, reducing off-target effects, increasing metabolic stability, and on so on, we developed a novel cyclopropanesulfonamide derivative for the treatment of EGFRC797S mutation in non-small cell lung cancer. On the other hand, sulfonamide drugs are also widely used as anti-inflammatory and antibacterial drugs in clinical practice. Thus, we believe that the development of the EGFR inhibitors possessing cyclopropanesulfonamide moiety will lay a foundation for the treatment of the diseases.

In order to overcome the drug resistance challenge posed by the C797S mutation, the present study first obtained a cell line (Ba/F3 cells) stably expressing the EGFR C797S mutant, and synthesised the a series of novel cyclopropane-sulfonamide derivatives as $EGFR^{C797S}$ inhibitors. Among them, compound **5d** exhibited exceptional in vitro activity, with IC_{50} values of 1.37±0.03 nM and 1.13±0.01 nM for inhibiting the EGFR kinases $EGFR^{L858R/T790M/C797S}$ and $EGFR^{del19/T790M/C797S}$, respectively, and 18 nM and 25 nM for BAF3-$EGFR^{L858R/T790M/C797S}$ and BAF3-$EGFR^{del19/T790M/C797S}$ cancer cell lines, respectively. Molecular docking studies showed that **5d** binds to $EGFR^{L858R/T790M/C797S}$ proteins. Detailed investigation demonstrated that **5d** exerts its inhibitory effects by downregulating the expression of EGFR, m-TOR, and downstream signaling molecules. Furthermore, **5d** inhibits cell cycle progression by inducing DNA damage and induce apoptosis in C797S mutant cells. Following experiments verified that **5d** inhibited cell cycle in G2-M phase by inhibiting CyclinB1 and CDK1 expression, caused apoptosis by activating cleaved caspase-3. Additionally, we verified the safety and selectivity of **5d** in A549 and PC9 cells, suggesting that **5d** has a certain selective safety profile. Indeed, in the Baf3-$EGFR^{19del/T790M/C797S}$ mutant xenograft tumor model, **5d** alone showed significant antitumor activity and safety.

Therefore, this study successfully demonstrated that **5d** is a novel fourth-generation EGFR inhibitor for the treatment of $EGFR^{L858R/T790M/C797S}$ and $EGFR^{19del/T790M/C797S}$ mutated non-small cell lung cancer.

Conclusion

In summary, we designed and synthesized a series of novel cyclopropanesulfonamide derivatives as the $EGFR^{C797S}$ inhibitors. Among them, compound **5d** exhibited exceptional in vitro activity, with IC_{50} values of 1.37±0.03 nM and 1.13 ±0.01 nM for inhibiting the EGFR kinases $EGFR^{L858R/T790M/C797S}$ and $EGFR^{del19/T790M/C797S}$, respectively, and 18 nM and 25 nM for BAF3-$EGFR^{L858R/T790M/C797S}$ and BAF3-$EGFR^{del19/T790M/C797S}$ cancer cell lines, respectively. Mechanistic study revealed that **5d** exerts its inhibitory effects by downregulating the expression of EGFR, m-TOR, and downstream signaling molecules, hindered cellular DNA damage repair. Additionally, **5d** induced cancer cell apoptosis by activating the expression of the apoptosis-related protein. Overall, the results of the present study demonstrate that **5d** is a good lead molecule for the development of fourth-generation EGFR inhibitors and is worth further investigation.

Data Sharing Statement

All methods are reported in accordance with ARRIVE guidelines (https://arriveguidelines.org). All data generated or analysed during this study are included in this published article and its Supplementary Information files.

Ethics Approval and Consent to Participate

This study was approved by the Human Research Ethics Committee of Binzhou Medical University. In addition, studies describing reports involving live animals were conducted in accordance with the ARRIVE guidelines (PLoS Bio 8(6), e1000412,2010).

Acknowledgment

We thank the Shandong Provincial Natural Science Foundation (ZR2021QB172), National Natural Science Foundation of China (82103391, 32101019), the Key R&D Program of Shandong Province of China (2023CXPT012), BZMC Scientific Research Foundation (BY2020KYQD08, BY2019KYQD32) for financial support of this study.

Author Contributions

Mengxuan Wang: Methodology, Data curation. Zhenhong Xia: Writing - Review & Editing. Wenyan Nie: Software, Formal analysis. Chunlong Wang: Formal analysis. Haoran Nie: Resources. Shuai Zhang: Formal analysis. Jiaqi Qiu: Investigation. Yang Yang: Writing – original draft, Supervision. Cuifang Yao: Visualization. Ling Xu: Writing – review & editing, Supervision, Funding acquisition. Baijiao An: Writing – review & editing, Project administration, Funding acquisition. All authors made a significant contribution to the work reported, whether that is in the conception, study design, execution, acquisition of data, analysis and interpretation, or in all these areas; took part in drafting, revising or critically reviewing the article; gave final approval of the version to be published; have agreed on the journal to which the article has been submitted; and agree to be accountable for all aspects of the work.

Disclosure

The authors report no conflicts of interest in this work.

References

1. Giaccone G, He Y. Current knowledge of small cell lung cancer transformation from non-small cell lung cancer. *Semin Cancer Biol*. 2023;94:1–10. doi:10.1016/j.semcancer.2023.05.006
2. Herbst RS, Morgensztern D, Boshoff C. The biology and management of non-small cell lung cancer. *Natur*. 2018;553(7689):446–454. doi:10.1038/nature25183
3. Brody H. Lung cancer. *Nature*. 2020;587(7834):S7. doi:10.1038/d41586-020-03152-0
4. Testa U, Castelli G, Pelosi E. Lung cancers: molecular characterization, clonal heterogeneity and evolution, and cancer stem cells. *Cancers*. 2018;10(8):248. doi:10.3390/cancers10080248
5. Fu K, Xie F, Wang F, Fu L. Therapeutic strategies for EGFR-mutated non-small cell lung cancer patients with osimertinib resistance. *J Hematol Oncol*. 2022;15(1):173. doi:10.1186/s13045-022-01391-4
6. Voldborg BR, Damstrup L, Spang-Thomsen M, Poulsen HS. Epidermal growth factor receptor (EGFR) and EGFR mutations, function and possible role in clinical trials. *Ann Oncol*. 1997;8(12):1197–1206. doi:10.1023/A:1008209720526
7. Li X, Cai W, Yang G, et al. Comprehensive analysis of EGFR-mutant abundance and its effect on efficacy of EGFR TKIs in advanced NSCLC with EGFR mutations. *J Thorac Oncol*. 2017;12(9):1388–1397. doi:10.1016/j.jtho.2017.06.006
8. Chmielecki J, Gray JE, Cheng Y, et al. Candidate mechanisms of acquired resistance to first-line osimertinib in EGFR-mutated advanced non-small cell lung cancer [published correction appears in nat commun. 2023 jun 1;14(1):3179]. *Nat Commun*. 2023;14(1):1070. doi:10.1038/s41467-023-35961-y
9. Lim SM, Fujino T, Kim C, et al. BBT-176, a novel fourth-generation tyrosine kinase inhibitor for osimertinib-resistant EGFR mutations in non-small cell lung cancer. *Clin Cancer Res*. 2023;29(16):3004–3016. doi:10.1158/1078-0432.CCR-22-3901
10. Muhsin M, Graham J, Kirkpatrick P. Gefitinib. *Nat Rev Drug Discov*. 2003;2(7):515–516. doi:10.1038/nrd1136
11. Sidaway P. Erlotinib effective in the neoadjuvant setting. *Nat Rev Clin Oncol*. 2018;15(11):654.
12. He J, Su C, Liang W, et al. Icotinib versus chemotherapy as adjuvant treatment for stage II-IIIA EGFR-mutant non-small-cell lung cancer (EVIDENCE): a randomised, open-label, Phase 3 trial. *Lancet Respir Med*. 2021;9(9):1021–1029. doi:10.1016/S2213-2600(21)00134-X
13. Gelatti ACZ, Drilon A, Santini FC. Optimizing the sequencing of tyrosine kinase inhibitors (TKIs) in epidermal growth factor receptor (EGFR) mutation-positive non-small cell lung cancer (NSCLC). *Lung Cancer*. 2019;137:113–122. doi:10.1016/j.lungcan.2019.09.017
14. Ricciuti B, Baglivo S, Paglialunga L, et al. Osimertinib in patients with advanced epidermal growth factor receptor T790M mutation-positive non-small cell lung cancer: rationale, evidence and place in therapy. *Ther Adv Med Oncol*. 2017;9(6):387–404. doi:10.1177/1758834017702820
15. Morgillo F, Della Corte CM, Fasano M, Ciardiello F. Mechanisms of resistance to EGFR-targeted drugs: lung cancer. *ESMO Open*. 2016;1(3):e000060. doi:10.1136/esmoopen-2016-000060
16. Tang J, Salama R, Gadgeel SM, Sarkar FH, Ahmad A. Erlotinib resistance in lung cancer: current progress and future perspectives. *Front Pharmacol*. 2013;4:15. doi:10.3389/fphar.2013.00015
17. Mukherji D, Spicer J. Second-generation epidermal growth factor tyrosine kinase inhibitors in non-small cell lung cancer. *Expert Opin Investig Drugs*. 2009;18(3):293–301. doi:10.1517/13543780902762843

18. Wecker H, Waller CF. Afatinib. *Recent Results Cancer Res*. 2018;211:199–215.
19. Westover D, Zugazagoitia J, Cho BC, Lovly CM, Paz-Ares L. Mechanisms of acquired resistance to first- and second-generation EGFR tyrosine kinase inhibitors. *Ann Oncol*. 2018;29(suppl_1):i10–i19. doi:10.1093/annonc/mdx703
20. An B, Liu J, Fan Y, et al. Novel third-generation pyrimidines-based EGFR tyrosine kinase inhibitors targeting EGFR T790M mutation in advanced non-small cell lung cancer. *Bioorg Chem*. 2022;122:105743. doi:10.1016/j.bioorg.2022.105743
21. Cross DA, Ashton SE, Ghiorghiu S, et al. AZD9291, an irreversible EGFR TKI, overcomes T790M-mediated resistance to EGFR inhibitors in lung cancer. *Cancer Discovery*. 2014;4(9):1046–1061. doi:10.1158/2159-8290.CD-14-0337
22. Wang Z, Yang JJ, Huang J, et al. Lung adenocarcinoma harboring EGFR T790M and in trans C797S responds to combination therapy of first-and third-generation EGFR TKIs and shifts allelic configuration at resistance. *J Thorac Oncol*. 2017;12(11):1723–1727. doi:10.1016/j.jtho.2017.06.017
23. Patel H, Pawara R, Ansari A, Surana S. Recent updates on third generation EGFR inhibitors and emergence of fourth generation EGFR inhibitors to combat C797S resistance. *Eur J Med Chem*. 2017;142:32–47. doi:10.1016/j.ejmech.2017.05.027
24. Roper N, Brown AL, Wei JS, et al. Clonal evolution and heterogeneity of osimertinib acquired resistance mechanisms in EGFR mutant lung cancer. *Cell Rep Med*. 2020;1(1):100007. doi:10.1016/j.xcrm.2020.100007
25. Jia Y, Yun CH, Park E, et al. Overcoming EGFR(T790M) and EGFR(C797S) resistance with mutant-selective allosteric inhibitors. *Nature*. 2016;534(7605):129–132. doi:10.1038/nature17960
26. Graham J, Muhsin M, Kirkpatrick P. Cetuximab. *Nat Rev Drug Discov*. 2004;3(7):549–550. doi:10.1038/nrd1445
27. To C, Jang J, Chen T, et al. Single and dual targeting of mutant EGFR with an allosteric inhibitor. *Cancer Discov*. 2019;9(7):926–943. doi:10.1158/2159-8290.CD-18-0903
28. Cooper AJ, Sequist LV, Lin JJ. Third-generation EGFR and ALK inhibitors: mechanisms of resistance and management [published correction appears in Nat Rev Clin Oncol. 2022 nov;19(11):744]. *Nat Rev Clin Oncol*. 2019;11:6343–6351.
29. Zhang S, Anjum R, Squillace R, et al. The potent ALK inhibitor brigatinib (AP26113) overcomes mechanisms of resistance to first- and second-generation ALK inhibitors in preclinical models. *Clin Cancer Res*. 2016;22(22):5527–5538. doi:10.1158/1078-0432.CCR-16-0569
30. Eno MS, Brubaker JD, Campbell JE, et al. Discovery of BLU-945, a reversible, potent, and wild-type-sparing next-generation EGFR mutant inhibitor for treatment-resistant non-small-cell lung cancer. *J Med Chem*. 2022;65(14):9662–9677. doi:10.1021/acs.jmedchem.2c00704
31. Liu Y, Lai M, Li S, et al. LS-106, a novel EGFR inhibitor targeting C797S, exhibits antitumor activities both in vitro and in vivo. *Cancer Sci*. 2022;113(2):709–720. doi:10.1111/cas.15229
32. Xu L, Xu B, Wang J, et al. Recent advances of novel fourth generation EGFR inhibitors in overcoming C797S mutation of lung cancer therapy. *Eur J Med Chem*. 2023;245(Pt 1):114900. doi:10.1016/j.ejmech.2022.114900
33. Lu X, Yu L, Zhang Z, Ren X, Smaill JB, Ding K. Targeting EGFRL858R/T790M and EGFRL858R/T790M/C797S resistance mutations in NSCLC: current developments in medicinal chemistry. *Med Res Rev*. 2018;38(5):1550–1581. doi:10.1002/med.21488
34. Fan Y, Li W, Nie W, et al. Novel dual-target kinase inhibitors of EGFR and ALK were designed, synthesized, and induced cell apoptosis in non-small cell lung cancer. *Molecules*. 2023;28(5):2006. doi:10.3390/molecules28052006
35. Dong H, Ye X, Zhu Y, et al. Discovery of potent and wild-type-sparing fourth-generation EGFR inhibitors for treatment of osimertinib-resistance NSCLC. *J Med Chem*. 2023;66(10):6849–6868. doi:10.1021/acs.jmedchem.3c00277
36. Kashima K, Kawauchi H, Tanimura H, et al. CH7233163 Overcomes Osimertinib-Resistant EGFR-Del19/T790M/C797S Mutation. *mol Cancer Ther*. 2020;19(11):2288–2297. doi:10.1158/1535-7163.MCT-20-0229
37. Hou J, Xu M, Gu H, et al. ZC3H15 promotes glioblastoma progression through regulating EGFR stability. *Cell Death Dis*. 2022;13(1):55. doi:10.1038/s41419-021-04496-9
38. Pandey N, Black BE. rapid detection and signaling of DNA damage by PARP-1. *Trends Biochem Sci*. 2021;46(9):744–757. doi:10.1016/j.tibs.2021.01.014
39. Juretschke T, Beli P. Causes and consequences of DNA damage-induced autophagy. *Matrix Biol*. 2021;100-101:39–53. doi:10.1016/j.matbio.2021.02.004